Volume 1 | Number 1 | Jan 2013 | Pages 1–100

Dalton
Transactions

An international journal of inorganic chemistry
www.rsc.org/dalton

ROYAL SOCIETY OF CHEMISTRY

ROYAL SOCIETY OF CHEMISTRY

www.rsc.org/dalton

ARTICLE TYPE

Computer-Assisted Designed "selenoxy-chinolin": New Catalytic Mechanism of GPx-like and inhibition of metal-free and metal-associated Aβ aggregation†

**Zhiren Wang, Yali Wang, Wenrui Li, Zonghua Luo, Yang Sun, Ling Huang,* Xingshu Li***

Using support from rational computer-assisted design, a novel series of hybrids (selenoxy-chinolin) designed by fusing the metal-chelating agent CQ and the antioxidant ebselen were synthesized and evaluated as multitarget-directed ligands. Most of the hybrids demonstrated significant ability to mimic 10 GPx, which highly consistent with prediction results of DFT studies for the selenenyl sulfide intermediates in the computational design. Using ^{77}Se, ^{1}H and ^{13}C NMR spectroscopy and high-resolution mass spectroscopy (HRMS), a novel catalytic mechanism, including a new selenium quinone active specie was first demonstrated. 2D NMR studies indicated that the typical hybrid has an effective interaction with Aβ. In addition, the optimal compound **12k** was found to possess an excellent ability to 15 scavenge peroxide, inhibition of self- and metal-induced Aβ aggregation, and the ability to disassemble preformed self- and metal-induced Aβ aggregates effectively. Furthermore, **12k** was able to penetrate the central nervous system (CNS) and did not exhibit any acute toxicity in mice at doses up to 2000 mg/kg. Overall, we demonstrated that hybrid **12k**, through rational structure-based computational design, represented a potential for development as therapeutic agents in AD.

Introduction

20　　Glutathione (GSH), a major endogenous enzyme-catalyzed antioxidant, which is present at high concentrations of 1-2 mM within the brain, plays a fundamental role in the detoxification of ROS and regulates the intracellular redox environment.[1-3] 25 Postmortem human studies have demonstrated that the mRNA levels of GPx, a mammalian selenoenzyme, which protects various organisms from oxidative damage by catalyzing the reduction of harmful peroxides in the presence of GSH or other thiol cofactor systems, was elevated in the hippocampus and 30 inferior parietal lobe of Alzheimer's disease (AD) patients.[4-6] Small-molecule organoselenium compounds, which mimic the function of the antioxidant selenoenzyme GPx, have been developed for the prevention of diseases such as AD and Parkinson's disease (PD).[7-14] Ebselen, a classic example of a GPx 35 mimic, exhibits numerous biological activities and has undergone phase III clinical trials as an anti-inflammatory agent (Fig. 1).[15, 16] In recent years, many ebselen analogs or derivatives have been designed and studied for development as highly efficient GPx mimics.[17-26]
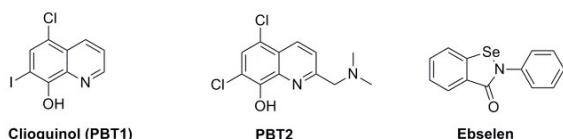
According to the "amyloid hypothesis", the production and accumulation of oligomeric aggregates of Aβ in the brain are central events in the pathogenesis of AD, and they are thought to 45 initiate the pathogenic cascade, ultimately leading to neuronal loss and dementia.[27, 28] Studies have indicated that remarkably high levels of biometals such as iron, zinc, and copper, which can bind to Aβ peptides and promote their aggregation,[29] were found in the brains of AD patients (Cu, 0.4 mM; Zn and Fe, 1 mM).[27] 50 Dysregulated redox-active metal ions bound or unbound to amyloid plaques resulted in concomitant free radical generation and reactive oxygen species (ROS) overproduction,[30] giving rise to neuronal death.[31-36] Thus, the modulation of these biometals in the brain has been proposed as a potential AD therapeutic 55 strategy. Clioquinol (CQ, Fig. 1) and its second-generation analog PBT2 (Fig. 1), a 8-hydroxyquinoline derivative with moderate affinity for Cu and Zn that inhibits metal-induced Aβ aggregation and reactive oxygen species generation, have been used for the treatment of AD and have showed evidence of 60 slowing cognitive deterioration and significantly decreasing plasma Aβ$_{1-42}$ levels.[37-39]

Considering the numerous biological activities of ebselen, especially its antioxidant and anti-inflammatory effects that were closely related to the etiology of AD,[16, 40] in this work, with 65 computer-assisted design, we fused the pharmacophores of CQ and ebselen into one molecule to obtain a "selenoxy-chinolin" with high GPx antioxidant ability, significantly inhibiting the activities of self-induced and metal-induced Aβ aggregation (Fig. 2). To date, the "selenoxy-chinolin" were, to the best of our

40 **Figure. 1**. Structures of clioquinol (PBT1), PBT2 and ebselen.

knowledge, the first single compounds obtained from computer-assisted design that target multipathogenic factors, including GPx, Aβ, metal ions and metal−Aβ, and remarkably improve their effects.
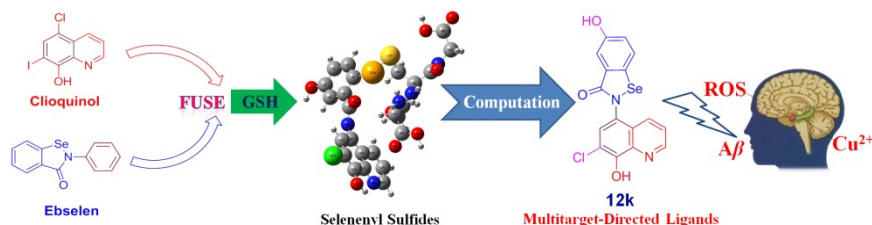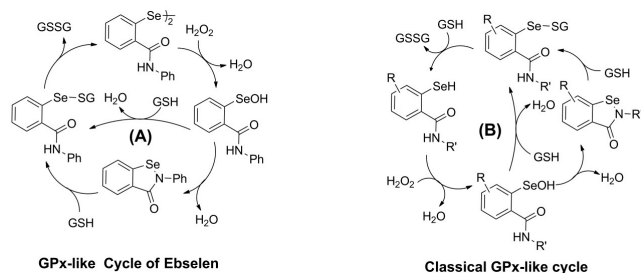

**Figure. 2**. Drug design strategy for multitarget-directed ligands

Results and discussion

Computation design and synthesis

Scheme 1. GPx-like cycle of ebselen (cycle A) and the classical GPx-like cycle (cycle B).

According to the classical GPx-like cyclic mechanism (Scheme 1), the weak intramolecular nonbonding Se $\cdots$ O interaction (lower positive charge on the selenium) in the selenenyl sulfide, resulted in low solvent-assisted proton exchange (SAPE) activation barrier,[41, 42] was favorable for the thiol to attack the sulfur in the selenenyl sulfide to obtain the selenol intermediate. On the contrary, due to the strong Se $\cdots$ O interaction (higher positive charge on the selenium), the attack of the thiol on the selenium in the selenenyl sulfide was more preferred and leaded to undesired thiol exchange, which was the rate-determining step of the classical GPx cycle (Scheme 2).[15, 21, 24, 26, 43]
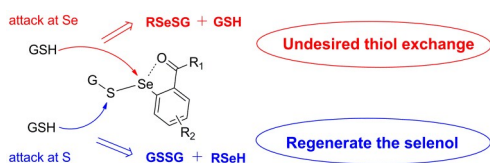
Scheme 2. The rate-determining step for the classical GPx-like catalytic cycle.

Therefore, identification of the proper substituent to attach to the A ring of the selenenyl sulfides to decrease the Se $\cdots$ O interaction and increase the positive charge on the sulfur atom was significant for strengthening the antioxidant potency of the organoselenium compounds.[21] We focused on introducing substituent groups at the *meta* or *para* positions of the A ring for reducing the Se $\cdots$ O interaction as many substituent groups, including coordinating substituents for seleninate esters,[44-46] *ortho* to the selenium on the benzene ring have been reported as GPx mimics.[18, 19, 21, 23, 24, 47]

DFT calculations were carried out to identify the proper substituent on the selenenyl sulfides, which were the crucial intermediates in the GPx-like cycle for the hybrids (see Supporting Information).[21, 47]

Table 1. Summary of DFT calculations and NBO analysis on the selenenyl sulfides at B3LYP/6-311+G(d,p) level on the B3LYP/6-311+G(d) level-optimized geometries.

| -	R	X	$r_{Se \cdots O}$ [Å]	$\theta_{O \cdots Se-S}$ [°]	q_{Se}	q_S	δ (^{77}Se NMR) (exptl) (ppm)[a]	$E_{Se \cdots O}$ [kcal mol^{-1}]
-	H	H	2.605	175.89	0.364	-0.032	553	11.41
R^1	Cl	H	2.619	174.69	0.371	-0.025	563	10.61
	CF$_3$	H	2.609	174.63	0.372	-0.021	564	11.11
	F	H	2.617	174.47	0.372	-0.027	568	10.75
	OMe	H	2.615	175.19	0.362	-0.029	562	11.32
R^2	Cl	H	2.630	174.06	0.365	-0.027	556	9.93
	F	H	2.635	173.80	0.360	-0.026	564	9.90
	OMe	H	2.616	175.47	0.355	-0.034	529	11.12
	OH	H	2.642	175.21	0.359	-0.030	529	8.48
R^1 = R^2	OMe		2.552	176.11	0.375	-0.047	563	14.76
R^3	F	H	2.511	176.27	0.388	-0.040	517	16.83
R^2	OH	Cl	2.646	173.40	0.351	-0.019	524	7.28
	OH	I[b]	2.618	175.40	0.358	-0.032	533	10.60

[a] Selenenyl sulfides dissolved in d_6-DMSO and Me$_2$Se as external (^{77}Se) standards [b] Using Lanl2dz as the basis set for the I atom and 6-311+G(d, p) for the other atoms.

The geometries were fully optimized using calculations at the B3LYP/6-311+g(d) level，which have been widely used to study the redox chemistry of small-molecule GPx mimics with high success.[15, 17-25, 47] The results in Table 1 showed that, without a substituent group, the selenenyl sulfides have a distance of 2.605 Å between the oxygen and selenium atoms, and 11.41 kcal mol^{-1} of O $\cdots$ Se orbital interaction energy. When a chloro group was introduced in the R^1 position, a slightly strong O $\cdots$ Se interaction energy (10.61 kcal mol^{-1}) was observed. However, replacement of the chloro group with both electron-withdrawing (trifluoromethyl, fluoro) and -donating (methoxy) groups gave a substantial increase in $E_{Se \cdots O}$ values of 11.11, 10.75 and 11.32 kcal mol-1, respectively. A shift of chloro, fluoro or methoxy from the R^1 to the R^2 position showed a drop of $E_{Se \cdots O}$ to 9.93, 9.90 and 11.12 kcal mol^{-1}, respectively. The results revealed that substituents at the *para* position, regardless of being electron-donating or -withdrawing, resulted in a lower interaction than those at the *meta* position of the A ring in selenenyl sulfides. This

could further be demonstrated by comparison the ^{77}Se NMR chemical shift of selenenyl sulfides in solution, the R^1 position substituted selenenyl sulfides (^{77}Se NMR: δ 563, 568, 562 ppm, respectively.) resulted in an apparent downfield shift of the ^{77}Se NMR chemical shift than the R^2 position (^{77}Se NMR: δ 556, 564, 529 ppm, respectively.). However, disubstituting the R^1 and R^2 positions with methoxy groups gave a greater interaction energy (14.72 kcal mol^{-1}) in comparison with only the R^2 position being substituted with a methoxy group (11.12 kcal mol^{-1}), which indicated that the effects of multiple methoxy groups were not cumulative and the result was in accordance with seleninate esters.[46] It is interesting that the replacement of the substituent at the *para* position (R^2) with a hydroxyl group led to a considerable decrease in the interaction energy (8.48 kcal mol^{-1}). Conversely, a shift of a fluoro group from the R^2 to the R^3 position provided a sharp increase in the $E_{Se \cdots O}$ value to 16.83 kcal mol^{-1}.

Next, we maintained R^2 as a hydroxyl group and modified the B ring of the quinoline moiety. The introduction of a chloro group showed a large decrease in $E_{Se \cdots O}$ (7.28 kcal mol^{-1}) and a significantly longer $r_{Se \cdots O}$ (2.646 Å) than in other selenenyl sulfides. A natural bond orbital (NBO) analysis further confirmed the weaker O $\cdots$ Se interaction in the selenenyl sulfides. The natural charge (+0.351) on the selenium was less positive and the charge on sulfur (–0.019) was more positive than in other selenenyl sulfides. In addition, the ^{77}Se NMR chemical shift of the selenenyl sulfide (^{77}Se NMR: δ 524) in solution was significant highfield compared with others. In contrast, replacement of a chloro group with an iodo group generated a moderate interaction energy (10.60 kcal mol^{-1}).

Synthesis
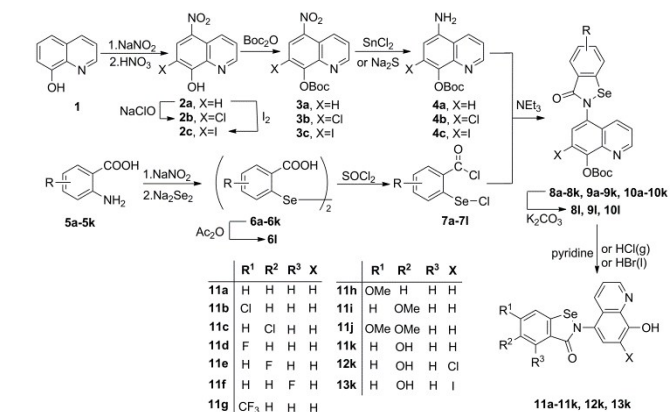
Scheme 3. Synthesis of **11a-11k**, **12k** and **13k**.

The target compounds **11a-11k**, **12k** and **13k** were obtained through the route described in Scheme 3. First, Compounds **2a-2c** and **3a** were prepared as reported in the literature.[14, 48, 49] Reduction of **3a** by SnCl₂ 2H₂O gave amine **4a**, and reduction of **3b** and **3c** with Na₂S 9H₂O in EtOH provided **4b** and **4c**, respectively. Na₂Se₂ was reacted with the corresponding benzenediazonium salts, which were prepared from the substituted 2-aminobenzoic acids and NaNO₂, to give the 2,2-diselenobisbenzoic acids **6a-6k** (intermediate **6l** was prepared by treating **6k** with acetic anhydride in pyridine). Subsequent reaction with SOCl₂ under reflux provided the 2-chloroselenobenzoyl chlorides **7a-7j**, which were reacted with the

corresponding amines in anhydrous CH₂Cl₂ to provide the key intermediates **8a-8k**, **9k** and **10k**. Treating **8k-10k** with K₂CO₃ in CH₃OH produced compounds **8l-10l**. Deprotection of the Boc group with piperidine gave the target compounds **11a-11c**, **11e**, and **11i-11j**. The hydrochloride salts **11d**, **11f-11g**, **11k**, **12k** and **13k** were obtained by removal of the Boc group with HCl gas. The hydrobromide salt of compound **11h** was prepared from intermediate **10h** by refluxing in HBr (47%).

Glutathione Peroxidase-Like Activity

The GPx-like activity of the clioquinol-ebselen hybrids was evaluated by the coupled reductase method, which uses GSH as the thiol cofactor and hydrogen peroxide (H₂O₂), *tert*-butyl hydroperoxide (*t*-BuOOH), and cumene hydroperoxide (Cum-OOH) as substrates.[17, 23, 24, 26]

Table 2. Initial rates, v_0 (μM·min^{-1}), for the reduction of hydroperoxides by GSH in the presence of CQ and ebselen hybrid derivatives.

	R¹	R²	R³	X		R¹	R²	R³	X
11a	H	H	H	H	11h	OMe	H	H	H
11b	Cl	H	H	H	11i	H	OMe	H	H
11c	H	Cl	H	H	11j	OMe	OMe	H	H
11d	F	H	H	H	11k	H	OH	H	H
11e	H	F	H	H	12k	H	OH	H	Cl
11f	H	H	F	H	13k	H	OH	H	I
11g	CF₃	H	H	H					

11a-11k, 12k, 13k

Comd.	GPx-like v_0 (μM.min^{-1}) ±SD [a]		
	H₂O₂	*t* BuOOH	Cum-OOH
11a	158.7 ±3.6	28.1 ±1.9	84.2 ±2.0
11b	148.3 ±1.6	28.9 ±0.4	93.7 ±2.6
11c	153.7 ±6.6	29.7 ±0.3	119.8 ±2.6
11d•HCl	132.8 ±2.6	26.1 ±0.7	95.43 ±1.6
11e	162.1 ±3.3	29.5 ±0.8	118.4 ±1.3
11f•HCl	249.3 ±5.2	27.2 ±0.8	180.9 ±1.6
11g•HCl	101.2 ±1.1	25.3 ±0.2	86.1 ±2.2
11h•HBr	88.6 ±4.2	17.3 ±1.4	46.5 ±0.7
11i	96.8 ±1.1	21.3 ±1.5	66.3 ±0.5
11j	74.53 ±1.2	16.2 ±0.9	49.1 ±0.3
11k•HCl	182.9 ±3.9	44.8 ±1.2	152.6 ±1.2
12k•HCl	236.0 ±3.7	70.0 ±1.6	198.2 ±10.2
13k•HCl	101.8 ±5.7	22.7 ±2.6	77.0 ±6.2
ebselen	124.3 ±4.3	27.7 ±0.4	62.3 ±2.0
clioquinol	37.8 ±2.0	4.5 ±0.2	6.3 ±0.4
control [b]	37.2 ±0.7	5.0 ±0.8	5.8 ±1.2

[a]Assay conditions: reactions were carried out in phosphate buffer (100 mM, pH 7.5) at 25 ℃ with 1 mM ethylene diamine tetraacetate (EDTA), 2 mM GSH, 0.4 mM NADPH, 1.3 unit/mL glutathione reductase (GR), 80 μM selenium compounds, and 1.6 mM peroxide. All values were determined in triplicate for the initial 10 s, and the average values with standard deviations were obtained. [b] Control values were obtained from the reduction of peroxide by GSH in the absence of compound.

The catalytic activities in Table 2 were in high accordance with the DFT calculations in all three peroxide systems. Compounds **11c** (chloro), **11e** (fluoro) and **11i** (methoxy), which contained a substituent *para* to the selenium atom, gave better catalytic activities than compounds **11b** (chloro), **11d** (fluoro) and **11h** (methoxy) where the substituent group was in the *meta* position. Compound **12k**, with a hydroxyl group *para* to the selenium atom, exhibited excellent activities (H₂O₂, v_0 = 236.0 μM min^{-1}; *t*-BuOOH, v_0 = 70.0 μM min^{-1}; Cum-OOH, v_0 = 198.2 μM min^{-1}), which could be attributed to the weakness of the Se $\cdots$ O noncovalent interaction (7.28 kcal mol^{-1}) in the selenenyl sulfide intermediate (Table 1). This weakening of interaction

overcomes the undesired thiol exchange at the selenium and regenerates the catalytically active selenol. The outstanding activities of **12k** suggested that the hydroxyl group *para* to the selenium was indispensable for high GPx activity. Compounds **11k** (182.9 μM min⁻¹; 44.8 μM min⁻¹; 152.6 μM min⁻¹) and **12k**, with or without a chlorine atom on the quinoline moiety, exhibited significant higher catalytic activities than ebselen. However, compound **13k** (101.8 μM min⁻¹; 22.7 μM min⁻¹; 66.3 μM min⁻¹), with an iodine atom on the quinoline moiety, showed much lower GPx-like activity. These results were consistent with the DFT studies for selenenyl sulfide intermediates in the computational design. It is worth noting that compound **11f** (249.3 μM min⁻¹; 27.2 μM min⁻¹; 180.9 μM min⁻¹), which contains a fluorine atom on the benzoselenazol-3(2*H*)-one moiety (R^3), also showed excellent GPx-like activity.

Determining the Catalytic Parameters.

Kinetic experiments were conducted to further understand the catalytic behavior of **11f** and **12k**, which exhibit eminent GPx-like activities (Tables S1†–S18† and Fig. S2†–S19†).[23, 24] It could be observed from Fig. S1† that, with the increase in the concentration of GSH in the presence of catalysts and peroxide, there was a rapid increase in the initial rate at the beginning, followed by saturation kinetics. These results confirmed that compounds **11f** and **12k** followed typical saturation kinetics for native GPx.

The K_M values (Table 3) obtained for **11f** (0.76, 0.75 and 0.48 mM) and **12k** (0.30, 0.30 and 0.33 mM) were much smaller (especially **12k**) than those for the parent compound ebselen (1.05, 0.83 and 1.18 mM), suggesting that the weak O···Se interaction significantly prevented the undesired thiol exchange reactions in the selenenyl sulfide. The catalytic efficiency obtained at various thiol concentrations of **12k** (11.87, 3.13 and 8.42 mM⁻¹ min⁻¹) was more than five times greater than that of ebselen (2.23, 0.65 and 0.80 mM⁻¹ min⁻¹) and two times greater than that of **11f** (5.90, 1.05 and 4.78 mM⁻¹ min⁻¹). Similarly, the catalytic efficiency of **12k** (6.83, 1.46 and 5.28 mM⁻¹ min⁻¹)

observed at various peroxide concentrations was approximately five-fold as large as that of ebselen (2.10, 0.22 and 1.59 mM⁻¹ min⁻¹) and two times that of **11f** (2.99, 0.40 and 1.98 mM⁻¹ min⁻¹). The relative low η (catalytic efficiencies) values of **11f** relative to **12k** was due to the presence of a strong $E_{Se···O}$ in the selenenyl sulfide, which led to thiol exchange reactions rather than to selenol regeneration.

Table 3. Effect of peroxide and GSH concentrations on V_{max} (maximum velocities), K_M (Michaelis constants), k_{cat} (catalytic constants), and η (catalytic efficiencies) for ebselen, **11f** and **12k**.

Comd.	Peroxide	V_{max} (μM·min⁻¹)	K_M (mM)	k_{cat} (min⁻¹)	η (mM⁻¹ min⁻¹)
effect of peroxide concentration [a]					
ebselen	H₂O₂ [a]	222.71	1.32	2.78	2.10
	t-BuOOH [a]	58.55	3.33	0.73	0.22
	Cum-OOH [a]	141.44	1.11	1.77	1.59
11f·HCl	H₂O₂ [a]	473.93	1.98	5.92	2.99
	t-BuOOH [a]	195.31	6.08	2.44	0.40
	Cum-OOH [a]	523.56	3.30	6.54	1.98
12k·HCl	H₂O₂ [a]	251.25	0.46	3.14	6.83
	t-BuOOH [a]	113.12	0.96	1.41	1.46
	Cum-OOH [a]	266.67	0.63	3.33	5.28
effect of thiol concentration [b]					
ebselen	H₂O₂ [b]	187.96	1.05	2.35	2.23
	t-BuOOH [b]	43.01	0.83	0.54	0.65
	Cum-OOH [b]	75.64	1.18	0.95	0.80
11f·HCl	H₂O₂ [b]	361.01	0.76	4.51	5.90
	t-BuOOH [b]	62.77	0.75	0.78	1.05
	Cum-OOH [b]	184.16	0.48	2.30	4.78
12k·HCl	H₂O₂ [b]	284.90	0.30	3.56	11.87
	t-BuOOH [b]	74.68	0.30	0.94	3.13
	Cum-OOH [b]	222.71	0.33	2.78	8.42

[a] Assay conditions: reactions were carried out in phosphate buffer (100 mM, pH 7.5) at 25 ℃ containing 2 mM GSH, 0.4 mM NADPH, 1 mM EDTA, 1.3 U/mL GR, variable peroxide, and 80 μM test compound. [b] Assay conditions: reactions were carried out in phosphate buffer (100 mM, pH 7.5) at 25 ℃ containing variable GSH, 0.4 mM NADPH, 1 mM EDTA, 1.3 U/mL GR, 1.6 mM peroxide, and 80 μM test compound.

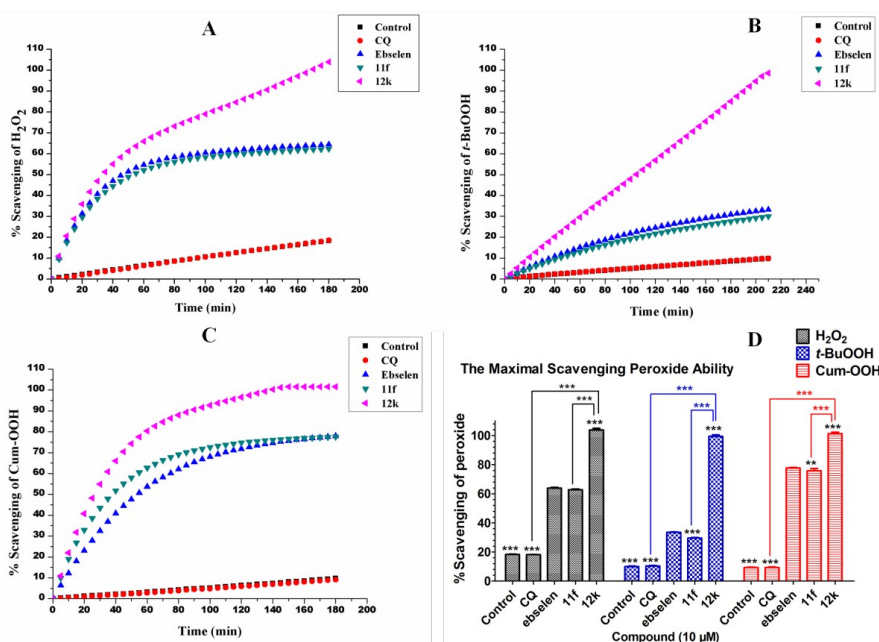**Scavenging peroxide in the presence of GSH catalyzed by clioquinol-ebselen hybrids**

Figure 3. Scavenging of peroxide by GSH over time in the presence and absence of catalyst. (A) Scavenging of H_2O_2. (B) Scavenging of t-BuOOH. (C) Scavenging of Cum-OOH. (D) The maximal scavenging peroxide ability. Assay conditions: reactions were carried out in phosphate buffer (100 mM, pH 7.5) at 25 ℃ with EDTA (1 mM), GSH (0.25 mM), NADPH (0.50 mM), GR (1.3 unit/mL), peroxide (0.20 mM) and catalyst (10 μM). Values reported are the means of three independent experiments. Statistical significance was analyzed by ANOVA: (∗∗) P < 0.01, (∗∗∗) P < 0.001.

To further evaluate the catalyzed antioxidant activity of clioquinol-ebselen derivatives, kinetic reactions in the presence of peroxide and GSH were conducted with ebselen and CQ as the controls (Fig. S20†−S34†). The results indicated that the full scavenging of H_2O_2, Cum-OOH and t-BuOOH was obtained within 180 - 210 minutes in the presence of catalyst **12k**, respectively (Fig. 3). In contrast, in the presence of **11f** and ebselen, less than 80% of the scavenging of H_2O_2 or Cum-OOH, and 35% of the scavenging of t-BuOOH, was achieved within 160 min (Fig. 3D), and the reaction did not proceed when the time was extended. This effects indicated that **12k**, unlike the parent compound ebselen, was capable of proceeding the GPx-like function at the concentration of diverse peroxide as low as possible, which has significant importance for protecting intracellular redox environment. All the results further show that the unique structure of hybrid **12k** results in significant antioxidant activities compared to the leading compounds ebselen and CQ.

Mechanism Study of the GPx-like Catalytic Cycle

To gain further insight into the activity differences among the hybrids with various substituents, a mechanistic study of the GPx-like catalytic cycle for the hybrids was carried out using ^{77}Se, ^{1}H and ^{13}C NMR spectroscopy and high-resolution mass spectroscopy (HRMS) (see Supporting Information).
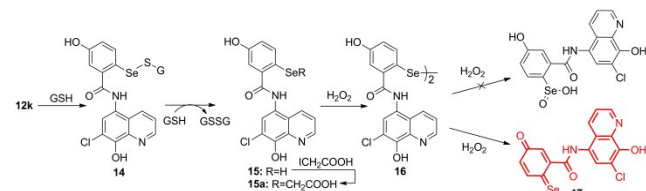

Scheme 4. Reaction of **12k** with GSH and H_2O_2.

As expected (Scheme 4), treatment of **12k** (^{77}Se NMR: δ 903 ppm) with one equivalent of GSH afforded selenenyl sulfide **14** (^{77}Se NMR: δ 524 ppm), which strongly suggested a weaker O ⋯Se intramolecular interaction compared to that of the selenenyl sulfide of ebselen (^{77}Se NMR: δ 545 ppm).[15] The addition of another equivalent of GSH to the solution produced selenol **15**, which was trapped by generating the selenide **15a** (^{77}Se NMR: δ 251 ppm) with iodoacetic acid and confirmed by HRMS (Fig. S35†−67†). Selenol **15** and its sodium selenolate (^{77}Se NMR: δ 158 ppm), obtained by reduction with NaBH$_4$, were not stable and were immediately oxidized to diselenide **16** (^{77}Se NMR: δ 432 ppm) in air. On the other hand, upon addition of H_2O_2 (1.0 equiv) and GSH (1.0 equiv) to a solution of selenenyl sulfide **14**, only a peak for diselenide **16** appeared, which indicated that the diselenide was the first product of the oxidation. Upon further addition of H_2O_2 (2.0 equiv), the peak for diselenide **16** disappeared and a signal for selenium quinone **17** (^{77}Se NMR: δ 803 ppm) appeared, which was further confirmed by ^{13}C NMR, ^{1}H NMR and HRMS (Fig. S49†−S53†). It was interesting that none of the other oxidative species, such as the selenenic or seleninic acids (expected δ: 1050-1350 ppm),[15, 18-21, 23-26, 50-52]

were detected when even more H_2O_2 was added to the reaction. This observation implies that the formation of selenium quinone **17** prevents the further oxidation of the selenium, and allows the nucleophilic attack of the thiol to be accelerated. Addition of GSH to diselenide **16** or selenium quinone **17** also produced selenenyl sulfide **14**. Taken together (Scheme 5), at a high concentration of GSH, selenol **15** was transformed into diselenide **16** and then reformed through selenenyl sulfide **14**. At a high concentration of hydrogen peroxide, diselenide **16** could be further oxidized to selenium quinone **17**. This observation was in precise accordance with the computational results for the selenenyl sulfide, which indicated that the structure of **12k** was different from the parent compound ebselen and was favorable for producing the catalytically active selenol rather than the disproportionation of selenenyl sulfide to generate diselenide, which was a characteristic feature GPx catalytic cycle of ebselen and its analogs.[15, 23, 26]

Nevertheless, for compound **11f** (^{77}Se NMR: δ 878 ppm), upon the addition of GSH (1 equiv), the new formed selenenyl sulfide (^{77}Se NMR: δ 517 ppm) underwent disproportionation to generate the corresponding diselenide (^{77}Se NMR: δ 455 ppm) immediately (Fig. S55†−S56†). This results demonstrated that **11f**, due to the strong Se ⋯O interaction presented in the selenenyl sulfide intermediate, has a same GPx-like mechanism with ebselen which enhanced the thiol exchange and facilitated disproportionation reaction.[15, 26] The facile disproportionation reaction could be responsible for the relative higher initial reduction rate of **11f** at high concentration of peroxide but unable to proceeding the GPx-like cycle at the concentration of diverse peroxide as low as possible.
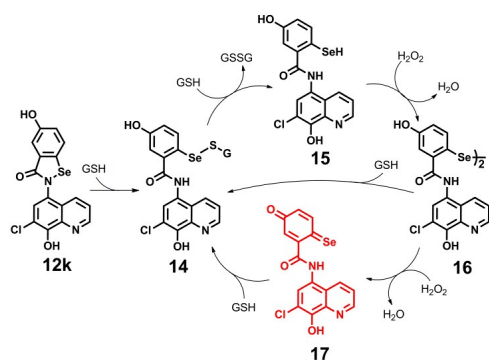
Scheme 5. Proposed catalytic cycle for the reduction of H_2O_2 by GSH in the presence of **12k**.

2D NMR Study of Hybrids with Aβ$_{1-42}$ in Solution

A 2D NMR study of **12k** with the monomeric form of Aβ$_{1-42}$ was performed,[53, 54] which significantly indicated the direct interactions of the hybrids with Aβ$_{1-42}$ from the chemical shift or broadening of the peaks of the Aβ$_{1-42}$ residues R5, H6, H14 and F20 upon treatment with a stoichiometric amount of **12k** (Fig. 4). As these residues were in close contact with the putative metal coordination site of Aβ (H6, H13, and H14),[55-57] these observations demonstrated that hybrid **12k** has not only a strong

bonding ability with the Aβ$_{1–42}$ monomer, but may also easily chelate metal ions in Aβ. With an excess of **12k** added to Aβ$_{1–42}$, remarkable chemical shift movements were detected because of

the possible change in the conformation of Aβ$_{1–42}$. Less peak movements were observed with methionine 35 (M35), suggesting that **12k** does not induce the oxidation of Aβ$_{1–42}$.[53]
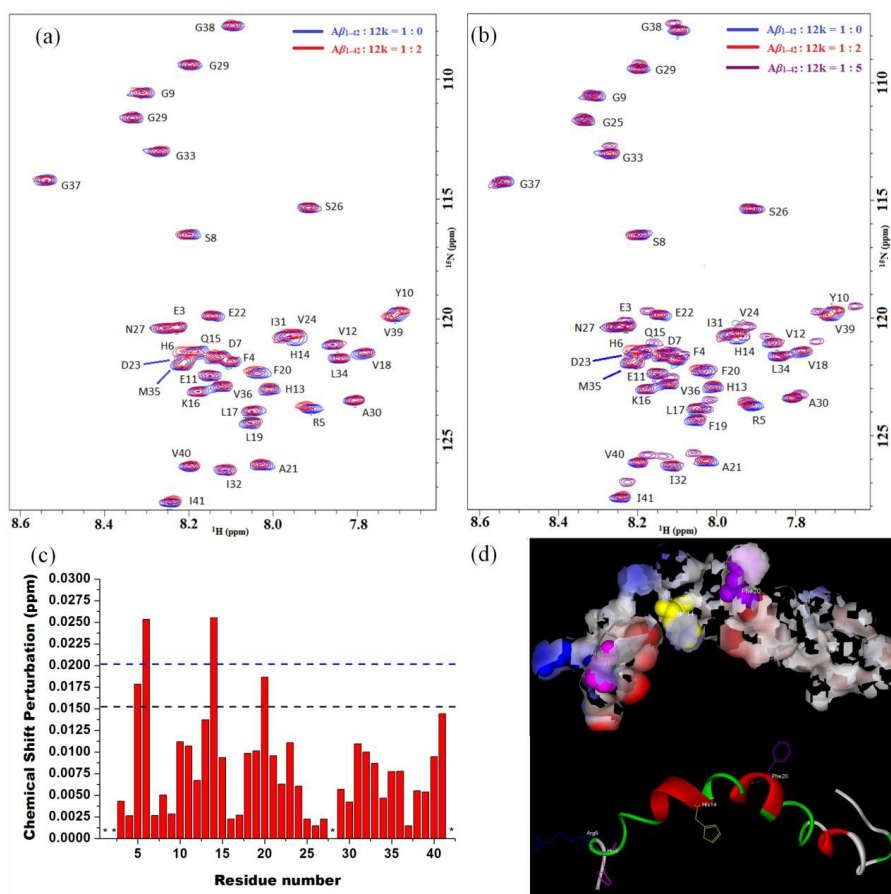

Figure. 4. Interactions of **12k** with Aβ$_{1–42}$ in solution. (a and b) 2D ^{1}H-^{15}N TROSY-HSQC NMR spectra of **12k**-titrated monomeric Aβ$_{1–42}$ (freshly dissolved Aβ$_{1–42}$ (50 μM) in 5 mM phosphate buffer, 0.5 mM Na$_2$EDTA, and 0.05 mM NaN$_3$, pH 7.5, 4 ℃, 950 MHz). (c) Chemical shift perturbations for Aβ$_{1–42}$ residues in the presence of **12k** (Aβ$_{1–42}$:**12k** = 1:2). * Denotes absent or overlapping signals. (d) Residues with the largest changes in chemical shifts mapped onto the structure of Aβ$_{1–42}$ (PDB 1Z0Q).
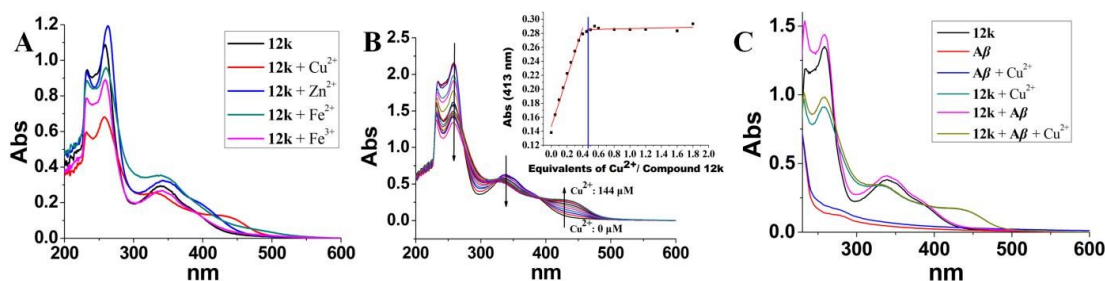

Figure 5. (A) UV absosobance spectrum of compound **12k** (50 μM) alone or in the presence of CuSO$_4$ (50 μM), ZnCl$_2$ (50 μM) or FeSO$_4$ (50 μM) in buffer (20 mM HEPES, 150 mM NaCl, pH 7.4). (B) UV-vis titration of compound **12k** with Cu^{2+} in buffer (20 mM HEPES, 150 mM NaCl, pH 7.4) at room temperature. The concentration of Cu^{2+} varied from 0 to 144 μM. A breakpoint was observed at 0.5:1 ratio. The concentration of compound **12k** was 80 μM. (C) UV absosobance spectrum of compound **12k** (50 μM) alone or in the presence of Cu^{2+} (25 μM) and Aβ$_{1–42}$ (25 μM) in buffer (20 mM HEPES, 150 mM NaCl, pH 7.4).

Metal Chelating Properties of Compounds

The ability of target compounds to chelate biometals such as Cu(II), Zn(II), Fe(II) and Fe(III) was studied by UV-visible spectrometry. New optical bands were observed in the UV-vis spectra for compounds **11k**, **12k** and **13k** upon the addition of CuSO$_4$ or ZnCl$_2$ and FeSO$_4$, suggesting that these compounds were able to interact with Cu^{2+}/Zn^{2+}/Fe^{2+} to form complexes (Fig.

S68†–S70†). For example, upon incubation of CuSO$_4$ with ligand **12k** in buffer (Fig. 5A), the new optical bands (in the absence of Cu^{2+}, the UV-vis spectrum of compound **12k** showed an absorption maximum at 259 nm and a shoulder at 339 nm; when Cu^{2+} was added, a new band associated with the copper complex appeared at 413 nm) indicated complex formation via metal chelation. Interestingly, after the addition of FeCl$_3$, there was no

significant shift; however, the absorption decreased significantly, suggesting a possible interaction between the compound and Fe^{3+}. Furthermore, the maximum absorption of **12k** exhibited a significant shift from 259 nm to 263 nm when $ZnCl_2$ was added. Additionally, the absorption shoulder shifted from 339 nm to 334 nm when $FeSO_4$ was added, suggesting that **12k** binds Zn^{2+} and Fe^{2+}. A series of UV-vis spectra of compound **12k** titrated with Cu^{2+} were shown in Fig. 5B, and the binding stoichiometry of compound **12k** with Cu^{2+} was determined by following the absorption changes at 413 nm. The presence of an isosbestic point revealed the formation of a unique Cu^{2+}-**12k** complex (Fig.

5B), and titration analysis was consistent with a 1:2 Cu^{2+}/ligand molar ratio. To further confirm the components of the complex, high-resolution mass spectroscopy (Fig. S68) was carried out in solution, and the result was positive (HRMS: Calcd for [(**12k**)$_2$Cu–2H]$^{2-}$, 420.8924, found, 420.8943). The interaction of **12k** with Cu^{2+} was further investigated by UV-vis spectrum in the presence of $A\beta_{1-42}$ (Fig. 5C). When **12k** was added to the solutions containing $A\beta_{1-42}$ and Cu^{2+}, the optical changes were similar to the samples containing **12k** and Cu^{2+} alone, which demonstrated that hybrid **12k** preferentially bonds with Cu^{2+} in the presence of $A\beta_{1-42}$
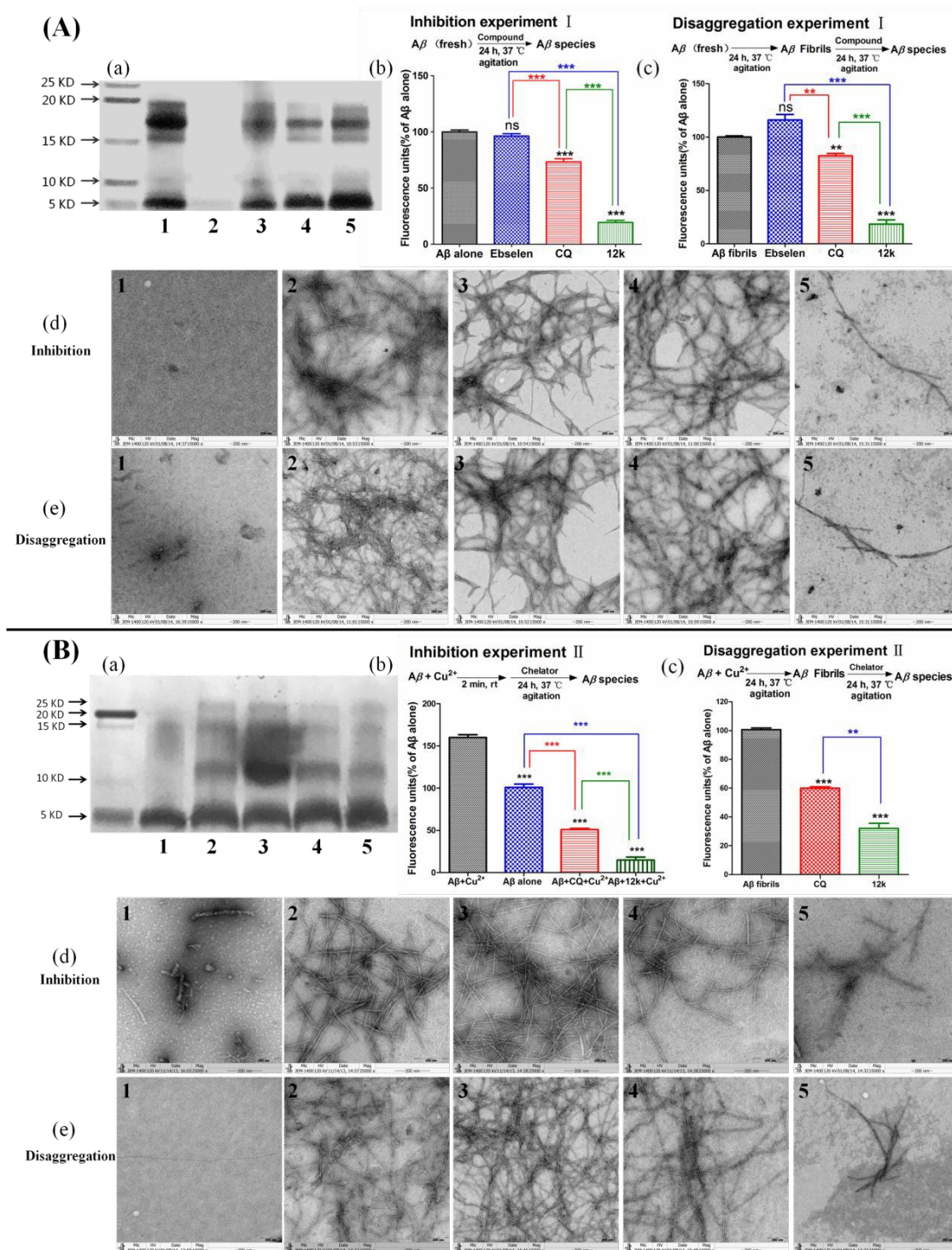
Figure 6. Experiments of inhibition and disaggregation in the presence of **12k**. (A) self-induced $A\beta_{1-42}$ aggregation experiments including (a) self-induced $A\beta_{1-42}$ species were visualized by PICUP, followed by tricine-SDS and silver staining. Lanes: (1) fresh $A\beta_{1-42}$, (2) $A\beta_{1-42}$ alone, (3) $A\beta_{1-42}$ + CQ, (4) $A\beta_{1-42}$ + ebselen, (5) $A\beta_{1-42}$ + **12k**. (b and c) Top: Scheme for the inhibition or disaggregation experiments. Bottom: The fluorescence intensity of the ThT binding assay. Statistical significance was analyzed by ANOVA: (∗∗) $p < 0.01$, (∗∗∗) $p < 0.001$. (d and e) TEM image analysis of the inhibition of $A\beta_{1-42}$
5 aggregation and disaggregation of $A\beta_{1-42}$ fibrils. Serial number: (1) fresh $A\beta_{1-42}$, (2) $A\beta_{1-42}$ alone, (3) $A\beta_{1-42}$ + CQ, (4) $A\beta_{1-42}$ + ebselen, (5) $A\beta_{1-42}$ + **12k.** Experimental conditions: $A\beta_{1-42}$ (25 μM); CQ, ebselen or **12k** (25 μM); PBS (50 mM); pH 7.4; 37 ℃. (B) Cu^{2+}-induced $A\beta_{1-42}$ aggregation experiments including (a) self-induced $A\beta_{1-42}$ species were visualized by gel electrophoresis. Lanes: (1) fresh $A\beta_{1-42}$, (2) $A\beta_{1-42}$ alone, (3) $A\beta_{1-42}$ + Cu^{2+}, (4) $A\beta_{1-42}$ + Cu^{2+} + CQ, (5) $A\beta_{1-42}$ + Cu^{2+} + **12k**. (b and c) Top: Scheme for the inhibition or disaggregation experiments. Bottom: The fluorescence intensity of the ThT binding assay. Statistical significance was analyzed by ANOVA: (∗∗) $p < 0.01$, (∗∗∗) $p < 0.001$. (d and e) TEM images analysis of the inhibition of
10 Cu^{2+}-induced $A\beta_{1-42}$ aggregation and disaggregation of Cu^{2+}-induced $A\beta_{1-42}$ fibrils. Serial number: (1) fresh $A\beta_{1-42}$, (2) $A\beta_{1-42}$ alone, (3) $A\beta_{1-42}$ + Cu^{2+}, (4) $A\beta_{1-42}$ + Cu^{2+} + CQ, (5) $A\beta_{1-42}$ + Cu^{2+} + **12k**. Experimental conditions: $A\beta_{1-42}$ (25 μM); $CuSO_4$ (25 μM); CQ, or **12k** (50 μM); HEPES (20 μM) and NaCl (150 μM); pH 6.6; 37 ℃.

Modulation of metal-free and meta-associated Aβ aggregation and disaggregation of Aβ

15   The ability of **12k** to inhibit the formation of $A\beta_{1-42}$ aggregates or to disassemble preformed $A\beta_{1-42}$ aggregates was investigated by gel electrophoresis (to visualize the changes in the size distribution of low molecular weight (LMW) $A\beta_{1-42}$ oligomers), a thioflavin-T (ThT) assay (to measure the formation
20 of Aβ aggregates) and transmission electron microscopy (TEM) (to determine the morphological changes in the Aβ species) (Fig. 6). As the results showed in Fig. 6A, $A\beta_{1-42}$ existed predominately as a mixture of monomers and oligomers of order 2-4 (Fig. 6Aa, lanes 1; Fig. 6Ad, sequence 1). In contrast,
25 monomers and oligomers were no longer detected and fibrils were the main form in the $A\beta_{1-42}$ sample after incubating for 24 h at 37 ℃. (Fig. 6Aa, lanes 2; Fig. 6Ad, sequence 2). Upon incubation of **12k** with the $A\beta_{1-42}$ sample, the intensity of the monomer band was strengthened remarkably and the oligomer
30 band was reduced substantially (Fig. 6Aa, lanes 5). However, the intensity of the monomer and oligomer bands in the $A\beta_{1-42}$ sample treated with CQ or ebselen was markedly reduced (Fig. 6Aa, lanes 3 and lanes 4). These results indicated that **12k** had a better ability to inhibit the self-induced $A\beta_{1-42}$ species aggregation
35 than CQ or ebselen. The results from gel electrophoresis were substantiated by the ThT assay (Fig. 6Ab and 6Ac) and TEM (Fig. 6Ad and 6Ae). The ThT assay showed that **12k** inhibited 84% (Fig. 6Ab) of the $A\beta_{1-42}$ aggregation and disaggregated 81% (Fig. 6Ac) of the preformed $A\beta_{1-42}$ aggregates. Comparatively, CQ
40 (32%; 18%) and ebselen (less than 10%) showed relatively less activity than **12k**. As observed by TEM, fewer Aβ fibrils were detected in the **12k**-treated Aβ sample (Fig. 6Ad and 6Ae, sequence 5) than in the controls (Fig. 6Ad and 6Ae, sequence 2), CQ (Fig. 6Ad and 6Ae, sequence 3) or ebselen (Fig. 6Ad and
45 6Ae, sequence 4), which further demonstrated that **12k** can attenuate Aβ aggregation and disassemble preformed Aβ aggregates effectively.

Furthermore, the capacity of **12k** to modulate Cu(II)-induced $A\beta_{1-42}$ aggregation and transform the preformed Cu(II)-induced
50 $A\beta_{1-42}$ aggregates was investigated (Fig. 6B). More Cu(II)-triggered $A\beta_{1-42}$ oligomers were observed in the presence of metal ions (Fig. 6Ba, lanes 3) than in the metal-free samples (Fig. 6Ba, lanes 2). On the other hand, upon incubation of $A\beta_{1-42}$ with Cu(II) and **12k**, the oligomerization was blocked almost
55 completely and the intensity of the monomer band increased significantly. (Fig. 6Ba, lanes 5). More importantly, **12k** (inhibition: 91%; disaggregation: 70%) demonstrated a greater effect on the control of Cu(II)-mediated Aβ aggregation and transformed Cu(II)-associated Aβ aggregates than CQ (68%; 41%)

60 in the ThT assay (Fig. 6Bb-6Bc). Consistent with the ThT binding assay results, the TEM images indicated that more well-defined Aβ fibrils (Fig. 6Bd and 6Be, sequence 3) were formed in the presence of Cu(II) compared with Aβ alone (Fig. 6Bd and 6Be, sequence 2), **12k** (Fig. 6Bd and 6Be, sequence 5) and CQ
65 (Fig. 6Bd and 6Be, sequence 4). These results revealed that **12k** could significantly modulate Cu(II)-induced $A\beta_{1-42}$ aggregation and disassemble the preformed Cu(II)-induced aggregates into relatively smaller, amorphous conformations. Taken together, all the inhibition and disaggregation results revealed that **12k**
70 possessed distinctive activity for the control of self- and Cu(II)-induced Aβ aggregation.

Blood-Brain Barrier Permeation Assay

To evaluate the brain penetration of the hybrids, the parallel artificial membrane permeability assay (PAMPA) was used as the
75 blood-brain barrier (PAMPA-BBB) assay, with a modification (Table S19†–S21†, Fig. S71†).[14] Compound **12k**, with a P_e value of 5.3×10^{-6} cm s^{-1}, would be able to penetrate the BBB and reach its biological targets in the CNS.

Compound 12k•HCl Demonstrated no Acute Toxicity

80   To evaluate the toxicity of **12k•HCl**, twenty KM mice (KM mice, which are common closed colony mice and most widely used in biomedical research in china) randomly allocated into 4 groups and the test compound **12k•HCl** was given in single oral doses of 0, 677, 1333, or 2000 mg/kg. After administration of the
85 compound, mice were monitored continuously for the first 4 h for any abnormal behavior and mortality changes, intermittently for the next 24 h, and occasionally thereafter for 14 days for the onset of any delayed effects. Durcing the experimental period, no acute toxicity, such as mortality, significant abnormal changes of
90 water or food consumption and body weight, were observed. Furthermore, all mice were sacrificed at the 14th day of drug administration and no damage to the heart, liver and kidneys were macroscopically detected. Overall, compound **12k•HCl** was non-toxic and well tolerated at doses up to 2000 mg/kg.

95 ## Conclusions

In summary, our study involved the computer-assisted design, synthesis, GPx-like activity evaluation and catalytic mechanism studies of a novel series of selenoxy-chinolin. The results indicated that the excellent GPx mimic activities of the hybrids,
100 including the eminent catalytic parameters and complete scavenging peroxide, which were highly consistent with that of the DFT studies. In contrast to the GPx-like mechanism of ebselen, a new GPx-like process has been demonstrated.

Especially, a new active species, selenium quinone, which prevented the further oxidation of the selenium and accelerated the nucleophilic attack of the thiol, was first reported and confirmed by ^{77}Se, ^{13}C, ^{1}H-NMR and HRMS. 2D NMR studies demonstrated that **12k** has an effective interaction with Aβ. Finally, other properties of the optimal compound **12k**, such as metal-chelating ligand and potential inhibitor of A$\beta_{1\text{-}42}$ aggregation, were also studied. This compound was able to penetrate the CNS, according to an in vitro blood-brain barrier model, and toxicity tests in mice showed that **12k** has no acute toxicity at doses up to 2000 mg/kg. All of these properties highlight the potential of compound **12k** as a lead compound for further study in treatment of AD.

Biological assays

ThT assay[58]

A$\beta_{1\text{-}42}$ (Millipore, counter ion: NaOH) was dissolved in ammonium hydroxide (1% v/v) to give a stock solution (2000 μM), which was aliquoted into small samples and stored at -80 ℃.

For the inhibition of self-mediated A$\beta_{1\text{-}42}$ aggregation experiment, the Aβ stock solution was diluted with 50 mM phosphate buffer (pH 7.4) to 50 μM before use. A mixture of the peptide (10 μL, 25 μM, final concentration) with or without the tested compound (10 μL) was incubated at 37 ℃ for 48 h. Blanks using 50 mM phosphate buffer (pH 7.4) instead of Aβ with or without inhibitors were also carried out. The sample was diluted to a final volume of 200 μL with 50 mM glycine–NaOH buffer (pH 8.0) containing thioflavin T (5 μM). Then the fluorescence intensities were recorded five minutes later (excitation, 450 nm; emission, 485 nm). The percent inhibition of aggregation was calculated by the expression (1-IF$_i$/IF$_c$) × 100% , in which IF$_i$ and IF$_c$ are the fluorescence intensities obtained for Aβ in the presence and absence of inhibitors after subtracting the background, respectively.

For the inhibition of copper-mediated A$\beta_{1\text{-}42}$ aggregation experiment, the Aβ stock solution was diluted in 20 μM HEPES (pH 6.6) with 150 μM NaCl. The mixture of the peptide (10 μL, 25 μM, final concentration) with or without copper (10 μL, 25 μM, final concentration) and the tested compound (10 μL, 50 μM, final concentration) was incubated at 37 ℃ for 24 h. Then 20 μL of the sample was diluted to a final volume of 200 μL with 50 mM glycine–NaOH buffer (pH 8.0) containing thioflavin T (5 μM). The detection method was the same as that of self-mediated A$\beta_{1\text{-}42}$ aggregation experiment.

For the disaggregation of self-induced Aβ fibrils experiment, the Aβ stock solution was diluted with 10 mM phosphate buffer (pH 7.4). The peptide (15μL, 50 μM) was incubated at 37 ℃ for 24 h. The tested compound (15μL, 50 μM) was then added and incubated at 37 ℃ for another 24 h. Then 20 μL of the sample was diluted to a final volume of 200 μL with 50 mM glycine–NaOH buffer (pH 8.0) containing thioflavin T (5 μM). The detection method was the same as above.

For the disaggregation of copper-induced Aβ fibrils experiment, the Aβ stock solution was diluted in 20 μM HEPES (pH 6.6) with 150 μM NaCl. The mixture of the peptide (10 μL, 25 μM, final concentration) with copper (10 μL, 25 μM, final concentration) was incubated at 37 ℃ for 24 h. The tested

compound (10μL, 50 μM, final concentration) was then added and incubated at 37 ℃ for another 24 h. Then 20 μL of the sample was diluted to a final volume of 200 μL with 50 mM glycine–NaOH buffer (pH 8.0) containing thioflavin T (5 μM). The detection method was the same as above.

Chemical cross-linking and determination of oligomer frequency distributions

The sample preparation was same as that for the ThT assay. Immediately after their preparation, Photo-induced cross-linking of unmodified proteins (PICUP) was performed as described previously.[59, 60] Briefly, 1 μL of 40 mM ammonium persulfate (APS, Aldrich) and 1 μL of 2 mM tris(2, 2'-bipyridyl)dichlororuthenium(II) (Ru(Bpy)) (alfa aesar) were added to 18 μL of 25 μM A$\beta_{1\text{-}42}$ sample in a clear PCR tube. The mixture was irradiated for 1 s with visible light and then quenched immediately by adding 4 μL of 1 M DTT which dissolved in Tricine sample buffer (Beyotime). Samples are then analyzed using 1.5 mm thick, 10-20% Tris-Tricine gradient gels and silver stained (Beyotime). Gels were analyzed using ImageJ. Reported values are from averaging of three separate gels.[61]

2D NMR spectroscopy

The interaction of monomeric A$\beta_{1\text{-}42}$ with **12k** was determined by Two-dimensional (2-D) Translational Relaxation Optimized Spectroscopy (TROSY) ^{1}H-^{15}N Heteronuclear Single Quantum Correlation (HSQC) NMR measurements by titrating a 50 μM solution of ^{15}N-labeled A$\beta_{1\text{-}42}$ with a 25 mM stock solution of **12k•HCl** in DMSO-d_6.[53, 54] The concentration of DMSO used for the each sample was lower than 1 % v/v (final concentration) so that the influence of DMSO on the spectrum of Aβ is minor,[62, 63] and the hydrochloride of **12k** was well solubilized (with no precipitation at 4 ℃) in the buffer which was used for the experiment. The ^{15}N-labeled A$\beta_{1\text{-}42}$ was purchased from rPeptide and stored at -80 ℃. One sample (1.0 mg) was predissolved in aqueous NaOH solution (1mM, pH = 10) in a 1:1 ratio (mg:mL) with sonication for 1 min at 4 ℃. The basic pH = 10 solution of the ^{15}N-labeled A$\beta_{1\text{-}42}$ peptides were diluted with a 4 ℃ potassium phosphate buffered solution (5 mM, pH 7.5) that containing 0.50 mM ethylenediamine tetraacetic acid (Na$_2$EDTA), and 0.05 mM NaN$_3$, verified to be pH 7.5 before the start of each titration. Each spectrum was obtained with 9.5 kHz and 2.7 kHz spectral width and 2048 and 256 complex data points in the ^{1}H and ^{15}N dimension, respectively, 96 scans per free induction decay, 1.0 s relaxation delay on a Bruker Avance 950 MHz spectrometer at 4 ℃. 2D data were processed using TOPSPIN 3.2 (from Bruker) and analyzed with Sparky version 3.113. ^{1}H-^{15}N HSQC peaks were assigned by comparison with literature values.[53-55, 64, 65] The normalized chemical shift perturbation were calculated from equation 1.[66]

$$\Delta\delta_{N-H} = \sqrt{\frac{(\Delta\delta_H)^2 + (0.2(\Delta\delta_N))^2}{2}} \quad (\text{eq 1})$$

TEM assay[67]

For the metal-free experiment, Aβ stock solution was diluted with a 10 mM phosphate buffer (pH = 7.4); for the copper-induced experiment, Aβ stock solution was diluted with 20 μM HEPES (pH = 6.6) and 150 μM NaCl. The sample preparation

was same as that for the ThT assay.

Aliquots (10 µL) of the samples were placed on a carbon-coated copper/rhodium grid for 2 min. Each grid was stained with uranyl acetate (1%, 5 µL) for 2 min. After draining off the excess staining solution, the specimen was transferred for imaging in a transmission electron microscope (JEOL JEM-1400). All compounds are solubilized in the buffer which was used for the experiment.

Coupled reductase assay.

The GPx-like activity of the organoselenium compounds was determined using a spectrophotometric method at 340 nm as described by Wilson et al.[68] The test mixture contained GSH (2 mM), EDTA (1 mM), glutathione reductase (1.3 unite/mL) and NADPH (0.4 mM) in 100 mM potassium phosphate buffer, pH 7.5. GPx samples (80 µM) were added to the test mixture at 25 ℃, and the reaction was initiated by the addition of H_2O_2 (1.6 mM). The initial reduction rates were calculated from the oxidation rate of NADPH at 340 nm. The initial reduction rate was determined at least 3 times and calculated from the first 5–10% of the reaction using 6.22 mM^{-1} cm^{-1} as the extinction coefficient for NADPH.

In vitro blood-brain barrier permeation assay

The blood-brain barrier penetration of compounds was evaluated using the parallel artificial membrane permeation assay (PAMPA) described by Di et al.[69] Commercial drugs were purchased from Sigma and Alfa Aesar. Porcine brain lipid (PBL) was obtained from Avanti Polar Lipids. The donor microplate (PVDF membrane, pore size 0.45 mm) and acceptor microplate were both from Millipore. The 96-well UV plate (COSTAR®) was from Corning Incorporated. The acceptor 96-well microplate was filled with 300 µL PBS/EtOH (7:3), and the filter membrane was impregnated with 4 µL PBL in dodecane (20 mg/mL). Compounds were dissolved in DMSO at 5 mg/mL and diluted 50-fold in PBS/EtOH (7:3) to a final concentration of 100 µg/mL. Then, 200 µL of the solution was added to the donor wells. The acceptor filter plate was carefully placed on the donor plate to form a sandwich, which was left undisturbed for 10 h at 25 ℃. After incubation, the donor plate was carefully removed, and the concentration of compounds in the acceptor wells was determined using the UV plate reader (Flexstation® 3). Every sample was analyzed at five wavelengths in four wells and in at least three independent runs. P_e was calculated by the following expression: $P_e = -V_d \times V_a/[(V_d+V_a)A \times t] \times \ln(1\text{-drug}_{acceptor}/\text{drug}_{equilibrium})$ where V_d is the volume of donor well; V_a, volume in acceptor well; A, filter area; t, permeation time; drug$_{acceptor}$, the absorbance obtained in the acceptor well; drug$_{equilibrium}$, the theoretical equilibrium absorbance. The results are given as the mean ± standard deviation. In the experiment, 13 quality control standards (Table S19) of known BBB permeability were included to validate the analysis set. A plot of the experimental data versus literature values gave a strong linear correlation, P_e (exp.) = 1.4574P_e (lit.) - 1.0773 (R^2 = 0.9427) (Figure S71). From this equation and the limit established by Di et al. (P_e (lit.) = 4.0×10^{-6} cm/s) for blood-brain barrier permeation, we concluded that compounds with a permeability greater than 4.7×10^{-6} cm/s could cross the blood-brain barrier (Table S20).

Acute toxicity

The procedures for acute toxicity study were followed the similar protocols in our previous studies.[70, 71] A total of 20 KM mice (KM mice, which are common closed colony mice and most widely used in biomedical research in china) (male, 22 days, 18-20 g) purchased from the laboratory animal center of Sun Yat-sen University (Guangzhou, China) were used to evaluate the acute toxicity of compound **12k•HCl**. Mice were maintained with a 12-h light/dark cycle (light from 07:00 to 19:00) at 20-22 ℃ with a 60-70% relative humidity. Sterile food and water were provided according to institutional guidelines. Prior to each experiment, mice were fasted overnight and allowed free access to water. Compound **12k•HCl** was suspension in 0.5% carboxymethyl cellulose sodium (CMC-Na) salt solution (677, 1333, and 2000 mg/kg) and given via oral administration according to the divided experimental groups. After the administration of the compounds, the mice were observed continuously for the first 4 h for any abnormal behavior and mortality changes, intermittently for the next 24 h, and occasionally thereafter for 14 days for the onset of any delayed effects. All animals were sacrificed on the 14th day after drug administration and were macroscopically examined for possible damage to the heart, liver, and kidneys.

Metal-chelating study

The chelating studies were performed with a UV-Vis spectrophotometer. All compounds are solubilized in the buffer which was used for the experiment. The absorption spectra of each compound (50 µM, final concentration) alone or in the presence of $CuSO_4$, $FeSO_4$, or $ZnCl_2$ (50 µM, final concentration) for 30 min in buffer (20 mM HEPES, 150 mM NaCl, pH 7.4) were recorded at room temperature.

For the stoichiometry of the compound-Cu^{2+} complex, a fixed amount of **12k** (80 µM) was mixed with growing amounts of copper ion (0-144 µM), and the difference UV-vis spectra were examined to investigate the ratio of ligand/metal in the complex.

Statistical analysis

The results are expressed as the mean ± SD of at least three independent experiments. Data were subjected to Student's *t* test or one-way analysis of variance (ANOVA) followed by Dunnett's test. *P* values less than 0.05 were accepted to indicate the significance.

Acknowledgements

Notes and references

School of Pharmaceutical Sciences, Sun Yat-sen University, Guangzhou 510006, China; For L. Huang: Tel.: +086-20-3994-3051; Fax: +086-20-3994-3051; e-mail: huangl72@mail.sysu.edu.cn ; For X. Sh. Li: Fax: +086-20-3994-3050; Tel.: +086-20-3994-3050; E-mail:
5 *lixsh@mail.sysu.edu.cn*

1. S. P. Raps, J. C. K. Lai, L. Hertz and A. J. L. Cooper, *Brain Res.*, 1989, **493**, 398-401.

15 2. C. L. Hammond, T. K. Lee and N. Ballatori, *J. Hepatol.*, 2001, **34**, 946-954.

3. R. Dringen, *Prog. Neurobiol*, 2000, **62**, 649-671.

4. C. Jacob, G. I. Giles, N. M. Giles and H. Sies, *Angew. Chem. Int. Edit.*, 2003, **42**, 4742-4758.

20 5. C. B. Pocernich and D. A. Butterfield, *Biochimica et Biophys. Acta*, 2012, **1822**, 625-630.

6. Michael Y. Aksenov, H. Michael Tucker, Prakash Nair, Marina V. Aksenova, D. Allan Butterfield, Steven Estus and W. R. Markesbery, *J. Mol. Neurosci.*, 1998, **11**, 151-164.

25 7. G. Mugesh, W.-W. du Mont and H. Sies, *Chem. Rev.*, 2001, **101**, 2125-2180.

8. K. P. Bhabak and G. Mugesh, *Acc. Chem. Res.*, 2010, **43**, 1408-1419.

9. G. Mugesh and H. B. Singh, *Chem. Soc. Rev.*, 2000, **29**, 347-357.

10. M. P. Rayman, *Lancet*, 2000, **356**, 233.

30 11. H. Tapiero, D. M. Townsend and K. D. Tew, *Biomed. Pharmacother.*, 2003, **57**, 134-144.

12. J. P. d. Magalhães and G. M. Church, *Exp. Gerontol.*, 2006, **41**, 1-10.

13. J. Nordberg and E. S. J. Arnér, *Free Radic. Biol. Med.*, 2001, **31**, 1287-1312.

35 14. Z. Wang, Y. Wang, W. Li, F. Mao, Y. Sun, L. Huang and X. Li, *ACS Chem. Neurosci.*, 2014, **5**, 952-962.

15. B. K. Sarma and G. Mugesh, *Chem. Eur. J.*, 2008, **14**, 10603-10614.

16. P. C. Trippier, K. Jansen Labby, D. D. Hawker, J. J. Mataka and R. B. Silverman, *J. Med. Chem.*, 2013, **56**, 3121-3147.

40 17. K. P. Bhabak and G. Mugesh, *Chem. Eur. J.*, 2007, **13**, 4594-4601.

18. K. P. Bhabak and G. Mugesh, *Chem. Eur. J.*, 2008, **14**, 8640-8651.

19. J. K. Pearson and R. J. Boyd, *J. Phys. Chem. A*, 2008, **112**, 1013-1017.

20. B. K. Sarma, D. Manna, M. Minoura and G. Mugesh, *J. Am. Chem. Soc.*, 2010, **132**, 5364-5374.

21. B. K. Sarma and G. Mugesh, *J. Am. Chem. Soc.*, 2005, **127**, 11477-11485.

22. K. Selvakumar, H. B. Singh and R. J. Butcher, *Chem. Eur. J.*, 2010, **16**, 10576-10591.

50 23. K. Selvakumar, P. Shah, H. B. Singh and R. J. Butcher, *Chem. Eur. J.*, 2011, **17**, 12741-12755.

24. V. P. Singh, H. B. Singh and R. J. Butcher, *Eur. J. Org. Chem.*, 2011, **28**, 5485-5497.

25. V. P. Singh, J.-f. Poon, R. J. Butcher and L. Engman, *Chem. Eur. J.*, 55 2014, **20**, 12563-12571.

26. K. Satheeshkumar and G. Mugesh, *Chem. Eur. J.*, 2011, **17**, 4849-4857.

27. G. G. Pepeu, M. G., *Curr. Alzheimer Res.*, 2009, **6**, 86-96.

28. J. Hardy, *J. Neurochem.*, 2009, **110**, 1129-1134.

60 29. A. I. Bush, *J. Alzheimer's Dis.*, 2008, **15**, 223-240.

30. X. Huang, C. S. Atwood, M. A. Hartshorn, G. Multhaup, L. E. Goldstein, R. C. Scarpa, M. P. Cuajungco, D. N. Gray, J. Lim, R. D. Moir, R. E. Tanzi and A. I. Bush, *Biochemistry*, 1999, **38**, 7609-7616.

31. A. I. Bush, *Trends Neurosci.*, 2003, **26**, 207-214.

65 32. K. J. Barnham and A. I. Bush, *Curr. Opin. Chem. Biol.*, 2008, **12**, 222-228.

33. S. C. Drew and K. J. Barnham, *Acc. Chem. Res.*, 2011, **44**, 1146-1155.

34. P. Faller, *ChemBioChem*, 2009, **10**, 2837-2845.

70 35. G. Casadesus, M. A. Smith, Z. Xiongwei, G. Aliev, A. D. Cash, K. Honda, R. B. Petersen and G. Perry, *J. Alzheimer's Dis.*, 2004, **6**, 165-169.

36. R. J. Castellani, K. Honda, X. Zhu, A. D. Cash, A. Nunomura, G. Perry and M. A. Smith, *Ageing Res. Rev.*, 2004, **3**, 319-326.

75 37. C. W. Ritchie, A. I. Bush, A. Mackinnon and et al., *Arch. Neurol.*, 2003, **60**, 1685-1691.

38. L. Lannfelt, K. Blennow, H. Zetterberg, S. Batsman, D. Ames, J. Harrison, C. L. Masters, S. Targum, A. I. Bush, R. Murdoch, J. Wilson and C. W. Ritchie, *Lancet Neurol.*, 2008, **7**, 779-786.

80 39. P. A. Adlard, R. A. Cherny, D. I. Finkelstein, E. Gautier, E. Robb, M. Cortes, I. Volitakis, X. Liu, J. P. Smith, K. Perez, K. Laughton, Q.-X. Li, S. A. Charman, J. A. Nicolazzo, S. Wilkins, K. Deleva, T. Lynch, G. Kok, C. W. Ritchie, R. E. Tanzi, R. Cappai, C. L. Masters, K. J. Barnham and A. I. Bush, *Neuron*, 2008, **59**, 43-55.

85 40. L. Xie, W. Zheng, N. Xin, J.-W. Xie, T. Wang and Z.-Y. Wang, *Neurochem. Int.*, 2012, **61**, 334-340.

41. S. Antony and C. A. Bayse, *Inorg. Chem.*, 2011, **50**, 12075-12084.

42. C. A. Bayse and A. Pavlou, *Org. Biomol. Chem.*, 2011, **9**, 8006-8015.

43. A. J. Mukherjee, S. S. Zade, H. B. Singh and R. B. Sunoj, *Chem. Rev.*, 90 2010, **110**, 4357-4416.

44. Y. Nakashima, T. Shimizu, K. Hirabayashi, F. Iwasaki, M. Yamasaki and N. Kamigata, *J. Org. Chem.*, 2005, **70**, 5020-5027.

45. D. J. Press, E. A. Mercier, D. Kuzma and T. G. Back, *J. Org. Chem.*, 2008, **73**, 4252-4255.

95 46. D. J. Press, N. M. R. McNeil, M. Hambrook and T. G. Back, *J. Org. Chem.*, 2014, **79**, 9394-9401.

47. G. Mugesh, A. Panda, H. B. Singh, N. S. Punekar and R. J. Butcher, *J. Am. Chem. Soc.*, 2001, **123**, 839-850.

48. N. B. Patel, J. C. Patel and S. H. Modi, *J. Saudi. Chem. Soc.*, 2011, 100 **15**, 167-176.

49. U. K. Mazumder, M. Gupta, S. Bhattacharya, S. S. Karki, S. Rathinasamy and S. Thangavel, *J. Enzyme. Inhib. Med. Chem.*, 2004, **19**, 185-192.

50. K. P. Bhabak and G. Mugesh, *Chem. Eur. J.*, 2009, **15**, 9846-9854.

105 51. V. Nascimento, E. E. Alberto, D. W. Tondo, D. Dambrowski, M. R. Detty, F. Nome and A. L. Braga, *J. Am. Chem. Soc.*, 2012, **134**, 138-141.

52. S. S. Zade, H. B. Singh and R. J. Butcher, *Angew. Chem. Int. Edit.*, 2004, **43**, 4513-4515.

110 53. L. Hou, H. Shao, Y. Zhang, H. Li, N. K. Menon, E. B. Neuhaus, J. M. Brewer, I.-J. L. Byeon, D. G. Ray, M. P. Vitek, T. Iwashita, R. A. Makula, A. B. Przybyla and M. G. Zagorski, *J. Am. Chem. Soc.*, 2004, **126**, 1992-2005.

54. K. Ono, L. Li, Y. Takamura, Y. Yoshiike, L. Zhu, F. Han, X. Mao, T. 115 Ikeda, J. Takasaki, H. Nishijo, A. Takashima, D. B. Teplow, M. G. Zagorski and M. Yamada, *J. Biol. Chem.*, 2012, **287**, 14631-14643.

55. L. Hou and M. G. Zagorski, *J. Am. Chem. Soc.*, 2006, **128**, 9260-9261.

56. J. Danielsson, R. Pierattelli, L. Banci and A. Graslund, *FEBS J*, 2007, 120 **274**, 46-59.

57. P. Faller and C. Hureau, *Dalton. Trans.*, 2009, DOI: 10.1039/B813398K, 1080-1094.

58. M. Rosini, E. Simoni, M. Bartolini, A. Cavalli, L. Ceccarini, N. Pascu, D. W. McClymont, A. Tarozzi, M. L. Bolognesi, A. Minarini, 125 V. Tumiatti, V. Andrisano, I. R. Mellor and C. Melchiorre, *J. Med. Chem.*, 2008, **51**, 4381-4384.

59. G. Bitan and D. B. Teplow, *Acc. Chem. Res.*, 2004, **37**, 357-364.

60. L. Pujadas, D. Rossi, R. Andres, C. M. Teixeira, B. Serra-Vidal, A. Parcerisas, R. Maldonado, E. Giralt, N. Carulla and E. Soriano, *Nat.* 130 *Commun.*, 2014, **5**, 3443.

61. P. A. Novick, D. H. Lopes, K. M. Branson, A. Esteras-Chopo, I. A. Graef, G. Bitan and V. S. Pande, *J. Med. Chem.*, 2012, **55**, 3002-3010.

62. J. J. Braymer, J. S. Choi, A. S. DeToma, C. Wang, K. Nam, J. W. Kampf, A. Ramamoorthy and M. H. Lim, *Inorg. Chem.*, 2011, **50**, 135 10724-10734.

63. S. Lee, X. Zheng, J. Krishnamoorthy, M. G. Saveleff, H. M. Park, J. R. Brender, J. H. Kim, J. S. Derrick, A. Kochi, H. J. Lee, C. Kim, A. Ramamoorthy, M. T. Bowers and M. H. Lim, *J. Am. Chem. Soc.*, 2014, **136**, 299-310.

64. Y. Yan, S. A. McCallum and C. Wang, *J. Am. Chem. Soc.*, 2008, **130**, 5394-5395.

65. Y. Yan and C. Wang, *J. Mol. Biol.,* 2006, **364**, 853-862.

66. S. S. Hindo, A. M. Mancino, J. J. Braymer, Y. Liu, S. Vivekanandan, A. Ramamoorthy and M. H. Lim, *J. Am. Chem. Soc.*, 2009, **131**, 16663-16665.

67. J.-S. Choi, J. J. Braymer, R. P. R. Nanga, A. Ramamoorthy and M. H. Lim, *Proc. Natl. Acad. Sci. U. S. A.*, 2010, **107**, 21990-21995.

68. S. R. Z. Wilson, P. A.; Huang, R. R. C.; Spector, A., *J. Am. Chem. Soc.*, 1989, **111**, 5936-5939.

69. L. Di, E. H. Kerns, K. Fan, O. J. McConnell and G. T. Carter, *Eur. J. Med. Chem.*, 2003, **38**, 223-232.

70. C. Lu, Y. Guo, J. Yan, Z. Luo, H.-B. Luo, M. Yan, L. Huang and X. Li, *J. Med. Chem.*, 2013, **56**, 5843-5859.

71. Z. Luo, J. Sheng, Y. Sun, C. Lu, J. Yan, A. Liu, H.-b. Luo, L. Huang and X. Li, *J. Med. Chem.*, 2013, **56**, 9089-9099.

Table of Contents graphic